

One RING to Rule Them All: Radon Sinogram for Place Recognition, Orientation and Translation Estimation

Sha Lu^{1*}, Xuecheng Xu^{1*}, Huan Yin², Rong Xiong¹ and Yue Wang^{1†}

Abstract—LiDAR-based global localization is a fundamental problem for mobile robots. It consists of two stages, place recognition and pose estimation, and yields the current orientation and translation, using only the current scan as query and a database of map scans. Inspired by the definition of a recognized place, we consider that a good global localization solution should keep the pose estimation accuracy with a lower place density. Following this idea, we propose a novel framework towards sparse place-based global localization, which utilizes a unified and learning-free representation, Radon sinogram (RING), for all sub-tasks. Based on the theoretical derivation, a translation invariant descriptor and an orientation invariant metric are proposed for place recognition, achieving certifiable robustness against arbitrary orientation and large translation between query and map scan. In addition, we also utilize the property of RING to propose a global convergent solver for both orientation and translation estimation, arriving at global localization. Evaluation of the proposed RING based framework validates the feasibility and demonstrates a superior performance even under a lower place density.

I. INTRODUCTION

LiDAR-based global localization is a fundamental problem for mobile robots, which enables the initialization of a navigation system, as well as loop closing in a SLAM system [1, 2]. The problem is highly challenging since it aims at searching the solution over the entire candidate pose space, i.e., every pose that the robot can move on the map, using only the current scan and a database of map scans. In addition, lightweight computation and storage are also desired due to the constrained resource, thus introducing specific requirements of both effectiveness and efficiency for global localization.

To address the problem, a great number of works take the strategy originated from visual localization [3, 4, 5] by dividing the problem into two phases: place recognition first and then pose estimation [6, 7, 8]. Place recognition identifies the place where the robot lies, while the pose estimation yields the accurate position and orientation of the robot based on the recognized place. Note that the recognized place serves as an intermediate role between the two phases. From the perspective of candidate pose space discretization, we consider the place as a coarse-level discrete cell, which ensures that the current pose is in this cell. In this context,

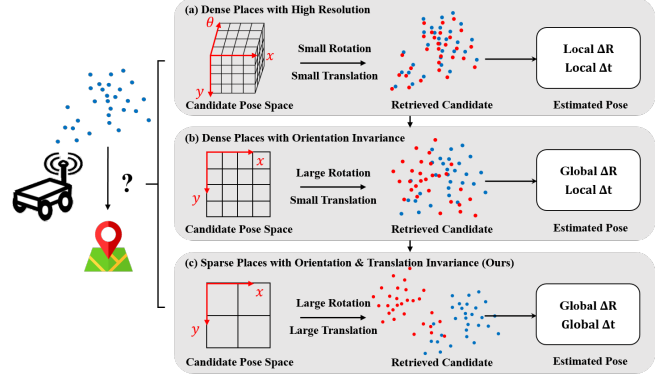


Fig. 1: Dense places and sparse places. We classify the global localization methods to two stages according to the map resolution. Our method aims at sparse places with orientation and translation invariance, as well as global convergent orientation and translations solvers.

a question of how to define the discretization resolution of a place naturally arises.

Imagining a spectrum aiming at this problem, one end represents *dense places* with high resolution, which means only a small subset of poses is regarded as a place. It simplifies the pose estimation as local convergence can be sufficient in a small cell. However, this design calls for high computation and storage given the dense discretization in all dimensions as shown in block (a) of Fig. 1. On the contrary, the other end represents *sparse places*, which infers a large area of the map, even the whole map, is regarded as one place. As a result, pose estimation becomes extremely difficult because it requires global convergence on the entire candidate pose space. Accordingly, the advantage of using sparse places is the lightweight computation and storage. In terms of global localization, we argue that only evaluation of place recognition may not fully reflect the performance of global localization. A more appropriate goal is to *keep the pose estimation accuracy with a lower place density*.

Based on the analysis above, some early existing works follow the idea of dense places [9, 10, 11]. These methods do not show very high computation. The reason is that robots in these scenarios usually travel along certain fixed trajectories, such as in-lane autonomous driving, which actually leads to reduced intrinsic dimensions of the candidate pose space. Nevertheless, in the case of general free space problems (the robot can move almost everywhere with arbitrary orientation, e.g., field robots in the wild), place recognition can be inefficient due to the irreducible candidate pose space. Therefore, recent studies like Scan Context [6] focuses on orientation

¹State Key Laboratory of Industrial Control and Technology, and the Institute of Cyber-Systems and Control, Zhejiang University, Hangzhou, 310058, China.

²Huan Yin is with the College of Design and Engineering, National University of Singapore, 119077, Singapore.

[†]Corresponding author wangyue@ipc.zju.edu.cn.

*Equal contribution.

invariance, which theoretically eliminates the dimension of orientation, leaving only the translation dimensions to be considered. These methods exponentially reduce the place density as shown in block (b) of Fig. 1. As a complement, global convergent orientation estimation is indispensable [6, 7, 8]. In this context, a further step to reduce the place density is to sparsify the translation space, which raises two critical challenges: place recognition robust to large relative orientation and translation, as well as efficient global convergence in both orientation and translation estimation.

Towards this goal, we propose a global localization solution as shown in block (c) of Fig. 1. We represent LiDAR scans in Radon sinogram (RING), which is very compact and allows for place recognition, orientation and translation estimation without additional feature engineering. The invariance of orientation and translation is theoretically derived for certifiable robustness and global convergence even under the large pose difference between current query scan and map scan, thus reducing the candidate pose space to sparse translation space. To the best of our knowledge, RING is the first learning-free unified representation to tackle all sub-tasks of global localization simultaneously. Experimental results validate RING in both place recognition and pose estimation, and show a superior global localization performance in more sparse place resolution. In summary, the contributions of this paper consist of:

- A novel framework towards sparse place-based global localization, which utilizes a unified representation, RING, for all sub-tasks.
- Theoretical derivation on orientation and translation invariance to achieve certifiable robustness and global convergence.
- Evaluation of the proposed method on three large-scale multi-session datasets. The experimental results show the feasibility and superior performance even under lower place density.

II. RELATED WORKS

For the place recognition task, numerous global point cloud descriptors have been proposed to represent the whole view of point cloud to achieve place description. These global descriptors can be categorized into handcraft descriptors and deep learning descriptors. Some of them can yield pose estimation at the same time.

A. Handcraft Descriptors

Early methods aggregate local features into a histogram and achieve the sparse encoding of a place. The common local features in computer vision community such as PFH [12], SHOT [13] and spin images [14] are explored. Other than those matured local features in the community, Magnusson et al. [1] utilized the surface orientation and smoothness to generate location histograms. Wohlkinger et al. [15] presented ESF which is a histogram of shape functions and Muhammad et al. [16] formed a histogram using normal vectors. Rohling et al. [9] proposed a histogram to describe the range distribution of the entire point cloud.

Other kinds of place recognition approaches rely on projections to reduce dimensionality. He et al. [17] presented M2DP, which projects a LiDAR scan to multiple 2D planes and extracts the density signature of points in each plane as a global descriptor. To further achieve rotation-invariance of the global descriptor, Kim et al. [6] proposed a rotation-invariant descriptor called scan context image. They adopted polar transformation on the point clouds and used the height information as the feature in a polar bin. Recently, Kim et al. [18] further enhanced the scan context image to achieve robustness to lateral/rotational changes.

B. Deep Learning Descriptors

The last decade witnessed increasingly rapid progress in feature extraction and classification, mainly backed up by advances in the area of deep learning. Employing a neural network to learn a compact descriptor of the point cloud allows for implicitly encoding and thus have more attractions than the handcrafted descriptors. Yin et al. [11] presented LocNet which firstly uses a 2D CNN after a handcrafted range histogram to enhance the place representation. Uy et al. [4] proposed PointNetVLAD which is a combination of two neural networks, a feature extractor, PointNet [19] and a feature aggregator, NetVLAD [10]. Furthermore, based on the handcrafted descriptor, scan context image, Kim et al. [20] introduced a CNN as a classifier for solving long-term place recognition problems. Cramariuc et al. [21] developed an approach that uses CNN to extract segments descriptors.

Intend to cover more in global localization, Schaupp et al. [22] proposed a system named OREOS for place recognition as well as orientation estimation. It uses a CNN as a feature extractor and a multilayer perceptron as an orientation estimator. Chen et al. [7] further utilized correlation head after a CNN as an orientation estimator. Xu et al. [8] adopted Fourier transform and differentiable phase correlation to achieve explicit rotation invariance in global descriptors.

III. PRELIMINARIES

A. Radon Transform

RING is the result of applying Radon transform to a 2D function $f(x, y)$. It is a integral transform of $f(x, y)$ along straight lines L , which projects a 2D function from the image space (x, y) to the parameter space (θ, τ) . Therefore, RING is denoted by $\mathcal{R}_f(L) = \mathcal{R}_f(\theta, \tau)$.

Scanning lines L are parameterized by θ and τ as:

$$x \cos \theta + y \sin \theta = \tau, (x, y) \in \mathbb{R}^2 \quad (1)$$

where θ is the incident angle between line L with the y axis and τ is the perpendicular distance from the origin to L . The range of θ is $[0, 2\pi)$ and the range of τ is $(-\infty, \infty)$. Then RING along a line is defined as

$$\begin{aligned} \mathcal{R}_f(\theta, \tau) &= \int_{x \cos \theta + y \sin \theta = \tau} f(x, y) dx dy \\ &= \int_{-\infty}^{\infty} \int_{-\infty}^{\infty} f(x, y) \delta(\tau - x \cos \theta - y \sin \theta) dx dy \end{aligned} \quad (2)$$

where $\delta(\cdot)$ is the Dirac delta function.

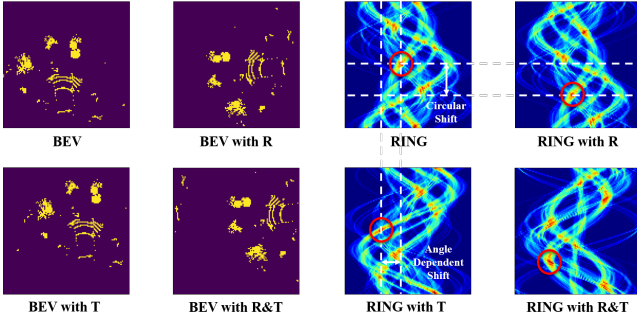


Fig. 2: Graphical illustration of orientation and translation properties of Radon Transform used in our method (R: Rotation, T: Translation). A rotation of point cloud corresponds to a circular column shift of RING. A translation of point cloud corresponds to an angle-dependent shift of RING.

B. Basic Properties

Translation: A translation of $f(x, y)$ by Δx and Δy in the image space results in a θ dependent shift s on τ axis of RING:

$$R_f(\theta, \tau) \rightarrow R_f(\theta, \tau - \Delta x \cos \theta - \Delta y \sin \theta) \quad (3)$$

Note that translation in image space actually causes a non-uniform change in the RING.

Orientation: An orientation of $f(x, y)$ by an angle α leads to a circular shift on θ axis of RING:

$$R_f(\theta, \tau) \rightarrow R_f(\theta + \alpha, \tau) \quad (4)$$

Compared to the image space translation, orientation change leads to uniform shift.

From (3) and (4), we can find that the translation and orientation of $f(x, y)$ is decoupled in the two variables τ and θ of RING. These properties help develop the invariance, which is beneficial for place recognition, as well as orientation and translation estimation.

IV. METHODOLOGY

Given a query scan P_Q and a database of map scans $\{P_D, T_D\}$ where T_D is the pose of P_D , the problem of global localization is to calculate the pose T_Q of P_Q . To address the problem, the proposed framework consists of three components. The LiDAR scan is firstly represented by RING. Then a translation invariant descriptor and an orientation invariant metric are built for place recognition, which retrieves a map scan P_D that is close to where P_Q is collected. Based on the retrieved map scan P_D , the relative orientation α and translation $[\Delta x, \Delta y]^T$ between P_Q and P_D is estimated, arriving at the final resultant global pose by compositing to T_D . Therefore, the goal is to keep the accuracy of estimated $\hat{\alpha}$ and $[\Delta \hat{x}, \Delta \hat{y}]^T$ by expanding the concept of ‘close’. The overview of our proposed framework is displayed in Fig. 3.

A. RING based Scan Representation

We follow the idea of ScanContext [6] to project the raw point cloud of a single scan into a bird-eye view representation (BEV). Instead of using the maximum height

of point cloud within a BEV grid, we remove the ground from the point cloud and only use the binary occupancy to represent whether there is a point cloud within the grid. Such representation is lightweight, and not affected by the different absolute heights of sensor and environment.

Volume to RING: We begin with voxelizing the ground removed point cloud, where the height axis of the volume is aligned with the vertical axis of the LiDAR sensor. Then we sum the voxels along the height dimension to reduce the volume to the occupancy BEV, which is regarded as the 2D function $f(x, y)$. Then we apply radon transform to $f(x, y)$, yielding RING based scan representation $R_f(\theta, \tau)$. In the sequel, RING of query scan is denoted as $R_Q(\theta, \tau)$, RING of map scan is denoted as $R_D(\theta, \tau)$.

B. Place Recognition

Given a query scan P_Q and a map scan P_D sharing the same place, we have the relationship between $R_Q(\theta, \tau)$ and $R_D(\theta, \tau)$ according to (3) and (4):

$$R_D(\theta, \tau) = R_Q(\theta + \alpha, \tau - \Delta x \cos(\theta + \alpha) - \Delta y \sin(\theta + \alpha)) \quad (5)$$

In practice, we cannot know the relative orientation and translation between the query scan and arbitrary map scan. So we build a translation invariant descriptor for the scan, and an orientation invariant metric to measure whether the two scans are acquired from the same place. Due to the limited scan range and overlapping, in order to decrease the place density, the invariance is expected to reserve under arbitrary α and as large τ as possible.

Translation invariant descriptor: In (3), a translation in BEV is projected to an angle-dependent shift in the variable of τ , which is shown in Fig. 2. To eliminate the effect of translation, we apply 1D discrete Fourier transform (DFT) on each row (τ axis) of RING and get the magnitude spectrum in the frequency domain. We define the resultant spectrum of RING as TI-RING. Denote query TI-RING and map TI-RING as M_Q and M_D respectively, the relationship between M_Q and M_D can be written as:

$$\begin{aligned} M_D(\theta, \tau) &= |\mathcal{F}(R_D(\theta, \tau))| \\ &= |\mathcal{F}(R_Q(\theta + \alpha, \tau - x \cos(\theta + \alpha) - y \sin(\theta + \alpha)))| \\ &= |\mathcal{F}(R_Q(\theta + \alpha, \tau))| = M_Q(\theta + \alpha, \tau) \end{aligned} \quad (6)$$

where $\mathcal{F}(\cdot)$ is the DFT operator. From (6), we notice that the relationship between M_Q and M_D is decoupled from the relative translation Δx and Δy . Such exact translation invariance is only affected by the limit scan range.

Orientation invariant similarity metric: In (4), an orientation shift in BEV is converted to a circular row shift in θ axis and it is decoupled with translation, which is depicted in Fig. 2 as well. In order to achieve orientation invariant metric for measuring similarity, we apply circular cross-correlation along the θ axis between M_Q and M_D as depicted in Fig. 4. The max correlation value of the circular cross-correlation results, denoted as $S(M_Q, M_D)$, is considered as the metric

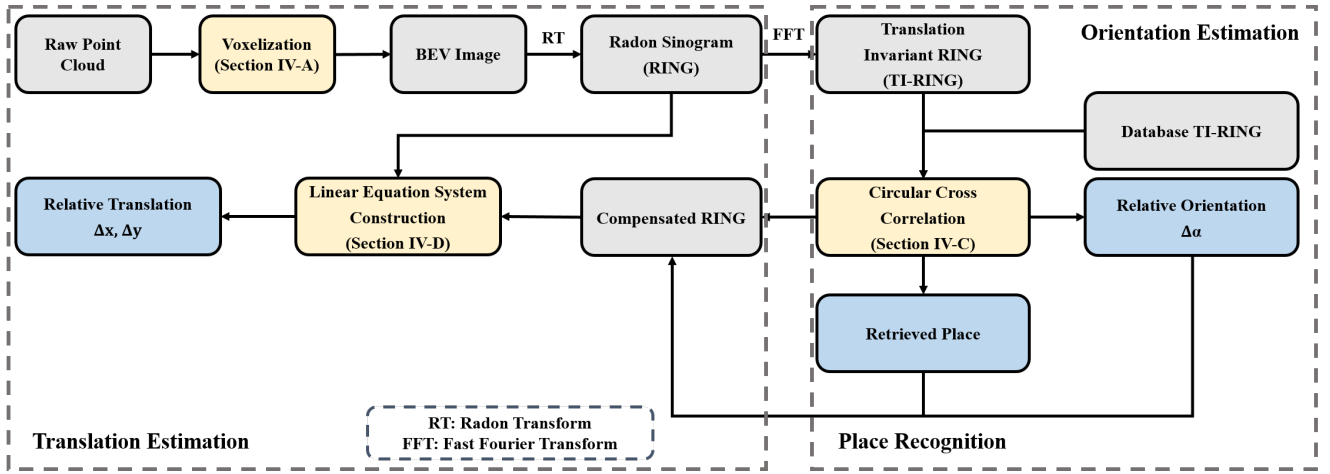


Fig. 3: Overview of the proposed framework about RING.

between the query scan P_Q and map scan P_D :

$$S(M_Q, M_D) = \max_{\alpha} \sum_{\theta_i} M_Q(\theta_i, \tau) \cdot M_D(\theta_i + \alpha, \tau) \quad (7)$$

where \cdot is the inner product. To increase the efficiency, we utilize the GPU-based fast Fourier transform (FFT) to compute the circular cross-correlation. By comparing the query TI-RING with map TI-RING using (7), we can find a most similar map scan which should be acquired in the same place with query scan.

Presence of large translation: Note that the TI-RING based similarity reserves the orientation invariance even larger relative translation presents, which is the main difference from previous methods that achieves orientation invariance with small relative translation [6, 7, 8]. This is an important step towards sparse and efficient global localization.

C. Orientation Estimation

As shown in (6), the relative orientation estimation between P_Q and P_D is equivalent to estimate the θ axis shift between M_Q and M_D , which can be completed by directly utilizing the TI-RING. Note that the optimal estimation $\hat{\alpha}$ of relative orientation is the one that achieves the maximum similarity metric (7):

$$\hat{\alpha} = \arg \max_{\alpha} \sum_{\theta_i} M_Q(\theta_i, \tau) \cdot M_D(\theta_i + \alpha, \tau) \quad (8)$$

Simultaneous solution: Note that orientation estimation is a by-product when solving place recognition, thus is solved very efficiently. Understandably, recognizing the correct place is coupled with estimating the correct orientation given that translation invariant descriptor is used.

D. Translation Estimation

After approximating the relative orientation $\hat{\alpha}$, we can use it to compensate the circular shift of map RING. The shifted map RING descriptor is denoted as $R'_D(\theta, \tau)$. Theoretically, if we apply inverse Radon transform to $R_D(\theta, \tau)$, the resultant BEV should only have a translation from the query

BEV. More specifically, the relationship between $R'_D(\theta, \tau)$ and $R_Q(\theta, \tau)$ becomes:

$$R'_D(\theta, \tau) = R_Q(\theta, \tau - x \cos(\theta + \alpha) - y \sin(\theta + \alpha)) \quad (9)$$

Linear equation system construction: Given the correct approximation i.e. $\hat{\alpha} \approx \alpha$, for each row pair of $R'_D(\theta, \tau)$ and $R_Q(\theta, \tau)$, we can get a linear equation according to (3) with unknowns Δx and Δy :

$$\Delta x \cos(\theta + \alpha) + \Delta y \sin(\theta + \alpha) = \Delta \hat{\tau} \quad (10)$$

where $\Delta \hat{\tau}$ is the optimal estimated shift between the paired row using the circular cross-correlation implemented by FFT as shown in Fig. 5. Assume the number of columns of a RING descriptor is k ($k = 120$ in our experiment). Then we have k linear equations with Δx and Δy as unknowns, which is an over-determined linear equation system:

$$\begin{bmatrix} \cos(\theta_1 + \alpha) & \sin(\theta_1 + \alpha) \\ \cos(\theta_2 + \alpha) & \sin(\theta_2 + \alpha) \\ \vdots & \vdots \\ \cos(\theta_k + \alpha) & \sin(\theta_k + \alpha) \end{bmatrix} \begin{bmatrix} \Delta x \\ \Delta y \end{bmatrix} = \begin{bmatrix} \Delta \hat{\tau}_1 \\ \Delta \hat{\tau}_2 \\ \vdots \\ \Delta \hat{\tau}_k \end{bmatrix} \quad (11)$$

Note that $\Delta \hat{\tau}$ varies for different θ_k . The noise in both estimations of α and $\Delta \tau$ can affect the equation coefficients, which leads to error in translation estimation.

Closed form: The translation estimation problem is converted to solve a linear equation system (11), which can be calculated in closed form, arriving at $[\Delta \hat{x}, \Delta \hat{y}]^T$.

V. EXPERIMENTAL RESULTS

In the experiments, we verify the performance of place recognition and pose estimation using the proposed method:

- validate the orientation and translation invariance of RING by testing the performance of place recognition at varied place density.
- validate the accuracy of pose estimation when the relative orientation and translation between the map and query scan are large.
- compare with other methods in terms of global localization success rate with respect to the place density.

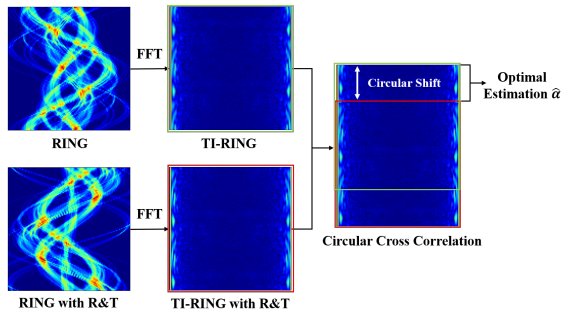


Fig. 4: Illustration of circular cross-correlation on TI-RING for orientation estimation (R: Rotation, T: Translation).

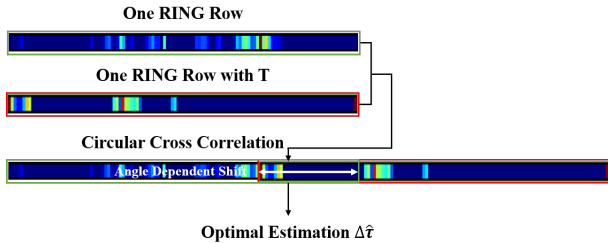


Fig. 5: Illustration of circular cross-correlation on RING for translation estimation (T: Translation).

A. Dataset and Experimental Settings

We utilize three large-scale datasets for evaluation: NCLT Dataset [23], MulRan Dataset [24] and Oxford Radar Robot-Car Dataset [25]. These datasets contain multiple sessions collected in different positions and orientations across various environmental conditions.

NCLT Dataset: NCLT Dataset is a large-scale and long-term dataset collected by a Segway robot at the University of Michigan North Campus. It consists of 27 sessions across four seasons, spaced approximately every two weeks for 15 months. To evaluate the multi-session place recognition, we use the trajectory collected on “2012-02-04” as the map data and other trajectories as the query data.

MulRan Dataset: MulRan Dataset comprises multimodal range data: Radar and LiDAR for robust structural place recognition algorithms. It is collected in multiple cities in different environments. In our experiments, we choose sessions from DCC and KAIST for place recognition evaluation.

Oxford Radar RobotCar Dataset: Oxford Radar Robot-Car Dataset provides optimised ground truth collected by Radar and two Velodyne HDL-32E LiDARs. We concatenate point clouds collected by the left and right LiDARs mounted on the vehicle to one single point cloud for evaluation.

On all datasets, the ROI of the LiDAR scan is cropped to $140m \times 140m$ centering at the sensor frame, and is represented by a 120×120 BEV with a resolution of $1.17m/pixel$ for RING extraction.

B. Comparative Methods

We mainly compare our method with four methods: M2DP [17], Fast Histogram [9], ScanContext [6], and ScanContext++ [18]. All methods are implemented using Python. The input of M2DP and Fast Histogram is the raw point cloud.

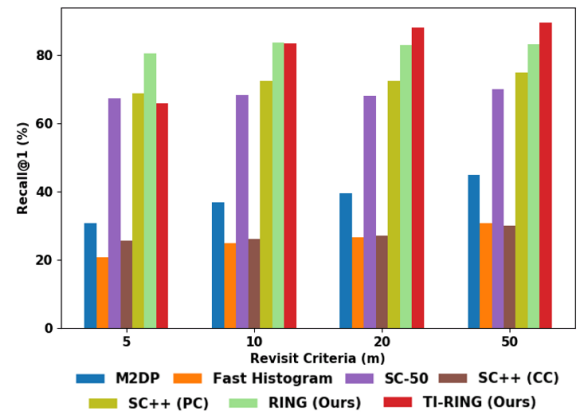


Fig. 6: Recall@1 vs. Revisit Criteria on NCLT dataset.

All parameters used in our experiments are the same as those in the original papers. The M2DP descriptor is a 192-length descriptor. The bucket count of Fast Histogram is set as 100. For a fair comparison, the resolution of SC and SC++ is the same as RING, which is 120×120 . The number of candidates of Scan Context is 50, keeping the same as the original paper.

C. Place Recognition Analysis

We first evaluate our method and other methods on place recognition performance with respect to different revisit criteria and place density. By changing the revisit threshold and place density, the translation and orientation invariance of the descriptor can be reflected.

Revisit criteria: Revisit criteria is the threshold determining whether the query pose and the map pose belong to the same place. To verify the invariance of our method, we first perform place recognition on two trajectories of NCLT dataset with respect to varied revisit criteria. We take “2012-02-04” sequence as map data and “2012-03-17” as query data. The map scans and query scans are sampled at fixed and equidistant intervals (map: $10m$, query: $5m$). The revisit criteria range from $5m$ to $50m$. Recall@1 is used as the evaluation metric shown in Fig. 6.

We notice that RING has competitive performance on all thresholds. The trend with respect to the revisit criteria is slightly smooth, which is similar to SC class methods. These results infer that the incorrectly recognized places are far away from the query pose. The trend of TI-RING is different, which lies a little lower than SC and RING under small threshold, but grows obviously with the increase of the threshold, and finally becomes the top. The underlying reason is the strong translation invariance of TI-RING, which is able to recognize places in a larger neighborhood. The other methods show lower performances, which may be explained by the discrimination capacity of the descriptors. Based on this result, we consider that our method is capable of handling place recognition with a lower place density.

Place density: We furthermore perform place recognition on NCLT dataset by changing the pose density i.e. the sampling interval along the map trajectory. The density is set to $10m$, $20m$, $50m$ and $100m$ respectively. All query data is sampled at a fixed $5m$ interval. The revisit threshold is taken

TABLE I: Place recognition on Oxford Dataset

Place density	Approach	Accuracy	F1 score	AUC
20m	TI-RING (Ours)	0.4973	0.8772	0.8878
	RING (Ours)	0.4863	0.8366	0.8787
	M2DP	0.2802	0.4496	0.4638
	Fast Histogram	0.0573	0.1181	0.0741
	SC-50	0.3317	0.5935	0.5366
	SC++ (PC)	0.3409	0.5967	0.5424
	SC++ (CC)	0.2361	0.3981	0.3710
50m	TI-RING (Ours)	0.4462	0.7295	0.7901
	RING (Ours)	0.3776	0.6131	0.6622
	M2DP	0.1681	0.3022	0.2650
	Fast Histogram	0.0444	0.0879	0.5312
	SC-50	0.2544	0.4639	0.4092
	SC++ (PC)	0.2589	0.4673	0.4096
	SC++ (CC)	0.1222	0.2211	0.1973

as one half of the density, which is $5m$, $10m$, $25m$ and $50m$. The results in Fig. 7 show that the performance of RING and TI-RING are a little higher than other methods at a density of $10m$. With the increase of density, our methods still maintain the top performance. While the performance of compared methods steeply drops, TI-RING, which is equipped with the translation invariance, only has a small drop from 0.6 to 0.4 at 100% recall. This result further validates that our method has strong robustness to larger relative translation between query and map poses.

Cross-dataset consistency: To validate the consistency of the performance, we further compare the methods on all three datasets with a place density of $20m$. For NCLT dataset, we select "2012-02-04" sequence as map data, "2012-05-26" and "2012-08-20" sequences as query data to evaluate place recognition performance. For MulRan dataset, we select DCC01/KAIST01 trajectory as map data, DCC02/KAIST02 trajectory as query data for evaluation. These sequences are relatively simple as low orientation and translation variance presents. For Oxford dataset, we choose two pairs "2019-01-11-13-24-51" to "2019-01-15-13-06-37" and "2019-01-11-13-24-51" to "2019-01-16-11-53-11". In this part, we choose precision-recall curve and F1 score-recall curve as the evaluation metric. Results with a place density of $50m$ are depicted in Fig. 8 to Fig. 10. Compared with other methods, TI-RING shows an obviously better performance, followed by RING, which is consistent on all datasets. As shown in Table I, we summarize the place recognition performance on Oxford dataset with two place density settings, $20m$ and $50m$. Accuracy is measured at 50% recall for comparison following [18]. The evaluated values of TI-RING are almost twice as the other methods for $50m$ place density. Moreover, the performance of our approach at $50m$ place density is almost 30% better than the best comparative methods at a smaller $20m$ place density, showing great improvement on sparse place based scenarios.

D. Pose Estimation Analysis

After place recognition, the downstream task is the pose estimation to gain the current robot pose. To perform pose estimation analysis, we choose NCLT dataset as the evaluation dataset ("2012-02-04" sequence acts as map data, other

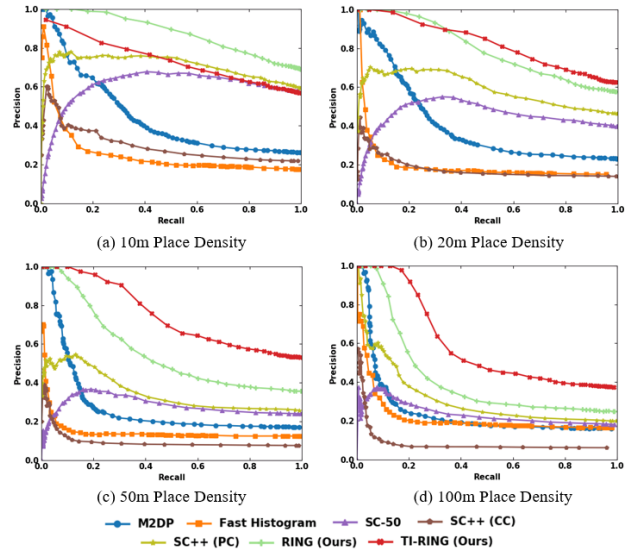


Fig. 7: Precision-recall curves at different map density on two sessions of NCLT dataset: 2012-02-04 (map) to 2012-03-17 (query).

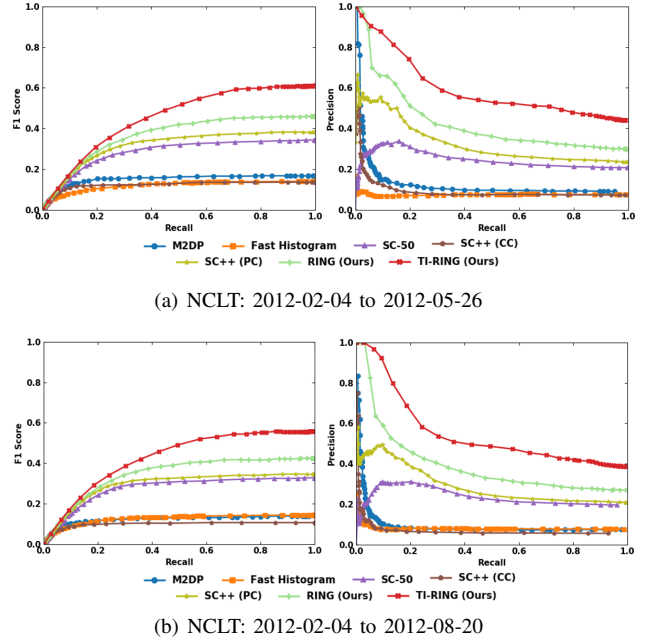
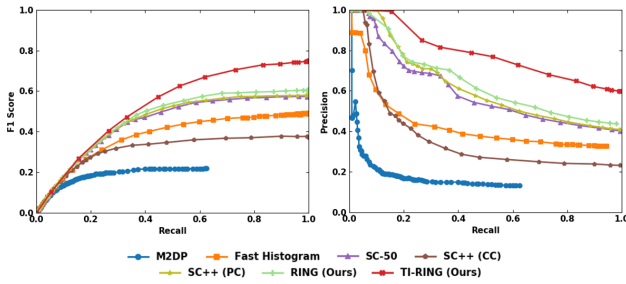


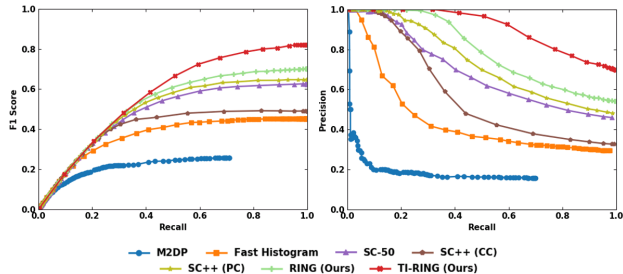
Fig. 8: F1 score-recall (left) and precision-recall (right) curves on NCLT dataset (50m place density).

sequences act as query data). Among the compared methods, only SC and SC++ can generate orientation. Therefore, we compare our method with SC and SC++. According to the pipeline proposed in Fig. 3, we estimate the relative orientation between two scans first. Then we compute the translation after compensating the orientation on RING. In this experiment, the pose estimation accuracy is only evaluated on scans of correctly recognized places.

Orientation and translation: The overall pose estimation results with respect to varied place density are shown in Fig. 11. For the orientation estimation, TI-RING has the lowest orientation estimation error. With the increase of place den-

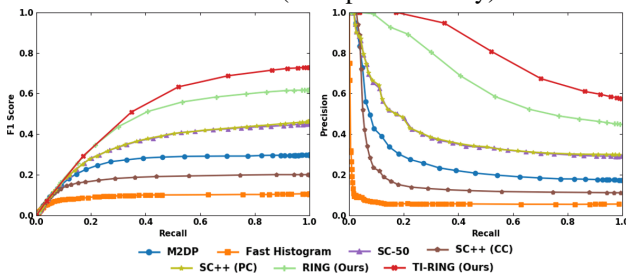


(a) MulRan: DCC01 to DCC02

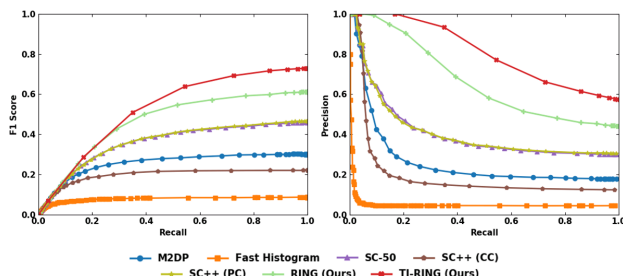


(b) MulRan: KAIST01 to KAIST02

Fig. 9: F1 score-recall (left) and precision-recall (right) curves on MulRan dataset (50m place density).



(a) Oxford: 2019-01-11-13-24-51 to 2019-01-15-13-06-37



(b) Oxford: 2019-01-11-13-24-51 to 2019-01-16-11-53-11

Fig. 10: F1 score-recall (left) and precision-recall (right) curves on Oxford dataset (50m place density).

sity, the estimation errors of all methods become larger while the pose estimation errors of TI-RING increase much slower than other methods. These results can be explained that the effect of relative translation is theoretically eliminated for TI-RING. For the lateral and longitudinal translation estimation, TI-RING demonstrates accuracy in about sub-meter level with place density lower than 20m. The inferior performance of RING is caused by the error of orientation estimation.

Stratified global localization success: Following the proposed goal of keeping the accuracy with a lower place

TABLE II: Translation, Orientation and Global localization success stratified by place density

Place density	Approach	Translation success rate	Orientation success rate	Localization success rate
20m	SC-50	0.2418	0.2364	0.0729
	SC++ (PC)	0.2382	0.2320	0.0667
	RING (Ours)	0.3404	0.3360	0.2373
	TI-RING (Ours)	0.5333	0.4453	0.3982
50m	SC-50	0.1493	0.0827	0.0409
	SC++ (PC)	0.1360	0.0800	0.0373
	RING (Ours)	0.1822	0.1413	0.1049
	TI-RING (Ours)	0.3956	0.2489	0.2258

density, we evaluate the accuracy by the number of all query scans that are correctly localized on the map. The threshold of correctness is set as 3° and $3m$. For SC and SC++, the relative translation is assigned by 0, which follows common practices that assigns the current pose by the pose of the recognized place. By aggregating the results from all datasets, a final performance comparison is shown in Table II. One can see that our method, TI-RING, rules place recognition, orientation estimation, and translation estimation at the same time. The margin over the comparative methods is obvious. Even with a place density of 50m, TI-RING outperforms the others with a place density of 20m, which means a superior accuracy is achieved with a smaller map.

VI. CONCLUSION

In this paper, we propose a unified descriptor named RING as the representation of a place. The RING descriptor can achieve certifiable orientation and translation invariance, resulting in further reduction the resolution of candidate map pose space. In the experiments, our method shows notable performance on place recognition, especially applied at lower place density. Based on the retrieved places, pose estimation can be further achieved at a relatively small error.

REFERENCES

- [1] Martin Magnusson et al. “Appearance-based loop detection from 3D laser data using the normal distributions transform”. In: *2009 IEEE International Conference on Robotics and Automation*. IEEE, 2009.
- [2] Renaud Dube et al. “SegMap: Segment-based mapping and localization using data-driven descriptors”. In: *The International Journal of Robotics Research* 39.2-3 (2020), pp. 339–355.
- [3] Stephanie Lowry et al. “Visual place recognition: A survey”. In: *IEEE Transactions on Robotics* 32.1 (2015), pp. 1–19.
- [4] Mikaela Angelina Uy and Gim Hee Lee. “Pointnetvlad: Deep point cloud based retrieval for large-scale place recognition”. In: *Proceedings of the IEEE conference on computer vision and pattern recognition*. 2018, pp. 4470–4479.
- [5] Simon Lynen et al. “Large-scale, real-time visual-inertial localization revisited”. In: *The International Journal of Robotics Research* 39.9 (2020).

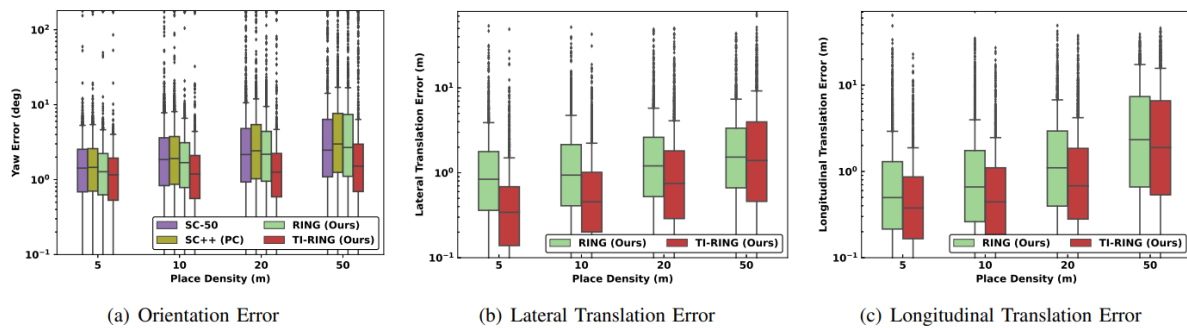


Fig. 11: Orientation and Translation Estimation Error on NCLT dataset.

- [6] Giseop Kim and Ayoung Kim. “Scan context: Ego-centric spatial descriptor for place recognition within 3d point cloud map”. In: *2018 IEEE/RSJ International Conference on Intelligent Robots and Systems (IROS)*. IEEE. 2018, pp. 4802–4809.
- [7] Xieyuanli Chen et al. “OverlapNet: Loop closing for LiDAR-based SLAM”. In: *arXiv preprint arXiv:2105.11344* (2021).
- [8] Xuecheng Xu et al. “Disco: Differentiable scan context with orientation”. In: *IEEE Robotics and Automation Letters* 6.2 (2021), pp. 2791–2798.
- [9] Timo Röhling, Jennifer Mack, and Dirk Schulz. “A fast histogram-based similarity measure for detecting loop closures in 3-d lidar data”. In: *2015 IEEE/RSJ International Conference on Intelligent Robots and Systems (IROS)*. IEEE. 2015, pp. 736–741.
- [10] Relja Arandjelovic et al. “NetVLAD: CNN architecture for weakly supervised place recognition”. In: *Proceedings of the IEEE conference on computer vision and pattern recognition*. 2016, pp. 5297–5307.
- [11] Huan Yin et al. “Locnet: Global localization in 3d point clouds for mobile vehicles”. In: *2018 IEEE Intelligent Vehicles Symposium (IV)*. 2018, pp. 728–733.
- [12] Radu Bogdan Rusu et al. “Aligning point cloud views using persistent feature histograms”. In: *2008 IEEE/RSJ international conference on intelligent robots and systems*. IEEE. 2008, pp. 3384–3391.
- [13] Samuele Salti, Federico Tombari, and Luigi Di Stefano. “SHOT: Unique signatures of histograms for surface and texture description”. In: *Computer Vision and Image Understanding* 125 (2014), pp. 251–264.
- [14] Andrew E Johnson and Martial Hebert. “Using spin images for efficient object recognition in cluttered 3D scenes”. In: *IEEE Transactions on pattern analysis and machine intelligence* 21.5 (1999), pp. 433–449.
- [15] Walter Wohlkinger and Markus Vincze. “Ensemble of shape functions for 3d object classification”. In: *2011 IEEE international conference on robotics and biomimetics*. IEEE. 2011, pp. 2987–2992.
- [16] Naveed Muhammad and Simon Lacroix. “Loop closure detection using small-sized signatures from 3D LIDAR data”. In: *2011 IEEE International Symposium on Safety, Security, and Rescue Robotics*. IEEE. 2011.
- [17] Li He, Xiaolong Wang, and Hong Zhang. “M2DP: A novel 3D point cloud descriptor and its application in loop closure detection”. In: *2016 IEEE/RSJ International Conference on Intelligent Robots and Systems (IROS)*. IEEE. 2016, pp. 231–237.
- [18] Giseop Kim, Sunwook Choi, and Ayoung Kim. “Scan context++: Structural place recognition robust to rotation and lateral variations in urban environments”. In: *IEEE Transactions on Robotics* (2021).
- [19] Charles R Qi et al. “Pointnet: Deep learning on point sets for 3d classification and segmentation”. In: *Proceedings of the IEEE conference on computer vision and pattern recognition*. 2017, pp. 652–660.
- [20] Giseop Kim, Byungjae Park, and Ayoung Kim. “1-day learning, 1-year localization: Long-term lidar localization using scan context image”. In: *IEEE Robotics and Automation Letters* 4.2 (2019), pp. 1948–1955.
- [21] Andrei Cramariuc et al. “Learning 3D segment descriptors for place recognition”. In: *arXiv preprint arXiv:1804.09270* (2018).
- [22] Lukas Schaupp et al. “OREOS: Oriented recognition of 3D point clouds in outdoor scenarios”. In: *2019 IEEE/RSJ International Conference on Intelligent Robots and Systems (IROS)*. 2019.
- [23] Nicholas Carlevaris-Bianco, Arash K Ushani, and Ryan M Eustice. “University of Michigan North Campus long-term vision and lidar dataset”. In: *The International Journal of Robotics Research* 35.9 (2016).
- [24] Giseop Kim et al. “Mulran: Multimodal range dataset for urban place recognition”. In: *2020 IEEE International Conference on Robotics and Automation (ICRA)*. IEEE. 2020, pp. 6246–6253.
- [25] Dan Barnes et al. “The oxford radar robotcar dataset: A radar extension to the oxford robotcar dataset”. In: *2020 IEEE International Conference on Robotics and Automation (ICRA)*. IEEE. 2020, pp. 6433–6438.

APPENDIX

A. Place recognition analysis

To compare the place recognition performance of the proposed method, we perform place recognition analysis on several sequences of three datasets. In addition to the experiments at $50m$ place density, we also conduct cross-dataset experiments at $20m$ place density. The results on the three datasets are shown in Fig. 12, Fig. 13 and Fig. 14. From the precision-recall curves and F1 score-recall curves, we can notice that the performances of all methods are better than that at $50m$ place density on the whole. With strong robustness to translation distribution, the place recognition performance of TI-RING decreases the least than other methods with the increase of place density. It demonstrates that the compared methods like Scan Context is only suitable for retrieving places at high place density, while our method has superior performance at low place density, which even outperforms the performances of other methods used at high place density. On MulRan dataset, the place recognition performances of all the methods are relatively high since the data collected in DCC and KAIST contains small rotation and lateral changes. On Oxford dataset, our method shows much better performance than other methods on the other two datasets. The underlying reason is that there exist several larger orientation and translation motions in terms of Oxford dataset, which deteriorate the overall place recognition performance to a great degree.

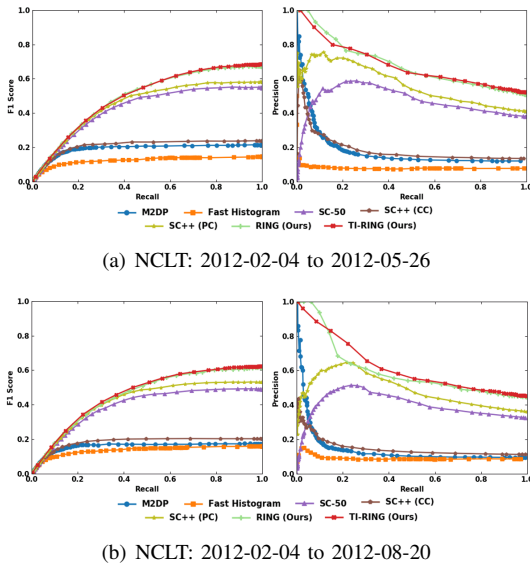
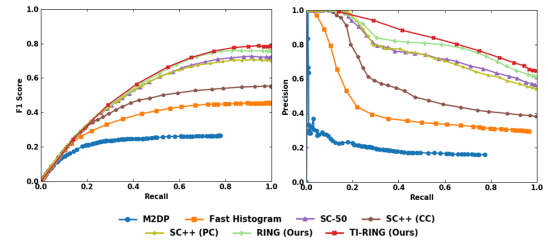
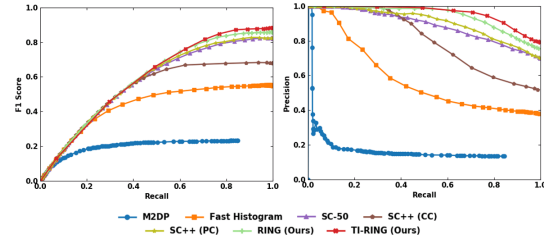


Fig. 12: F1 score-recall (left) and precision-recall (right) curves on NCLT dataset (20m place density).

As the second stage of global localization, pose estimation yields the relative pose between the query scan with the retrieved candidate scan. For evaluation of pose estimation performance of our method, we compare the pose estimation performance of our approach with Scan Context and Scan Context++ at two different place densities

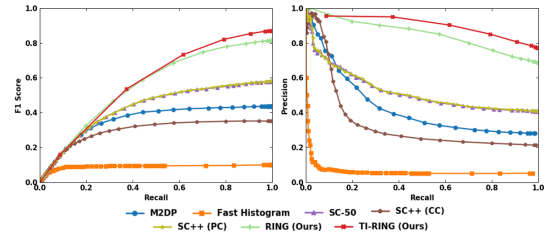


(a) MulRan: DCC01 to DCC02

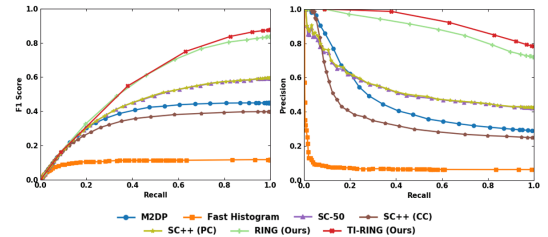


(b) MulRan: KAIST01 to KAIST02

Fig. 13: F1 score-recall (left) and precision-recall (right) curves on MulRan dataset (20m place density).



(a) Oxford: 2019-01-11-13-24-51 to 2019-01-15-13-06-37



(b) Oxford: 2019-01-11-13-24-51 to 2019-01-16-11-53-11

Fig. 14: F1 score-recall (left) and precision-recall (right) curves on Oxford dataset (20m place density).

($20m$ and $50m$) which are mainly used in our experiments. Using the evaluation metric described above, the results are depicted in Fig. 15 and Fig. 16. From the results of the four NCLT sequences, we can find that the success rates of both orientation and translation estimation of TI-RING shows substantially improvement on other methods at both $20m$ and $50m$ place density. This verifies the feasibility of our method for pose estimation at high place density. The success rates of estimated pose on the sequence collected later like "2012-08-20" are lower than that on the sequence collected earlier because the number of unseen places on the sequence collected later increases.

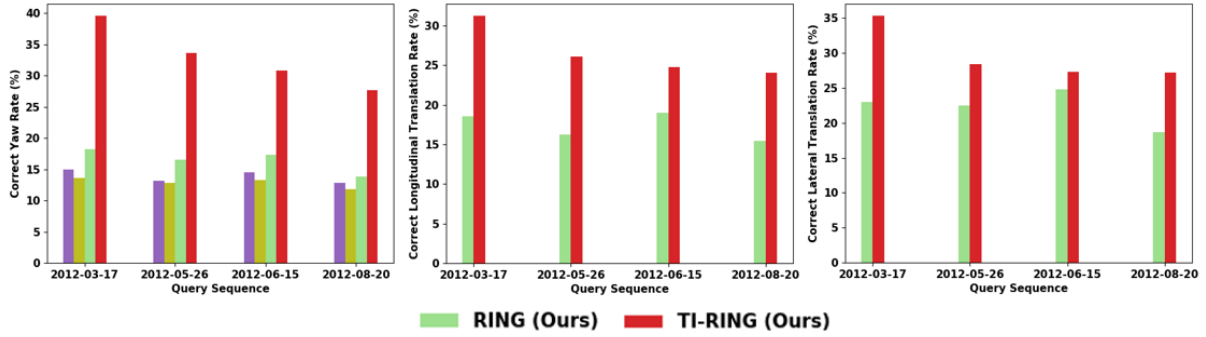


Fig. 15: Orientation and Translation Success Rate on NCLT dataset (20m place density).

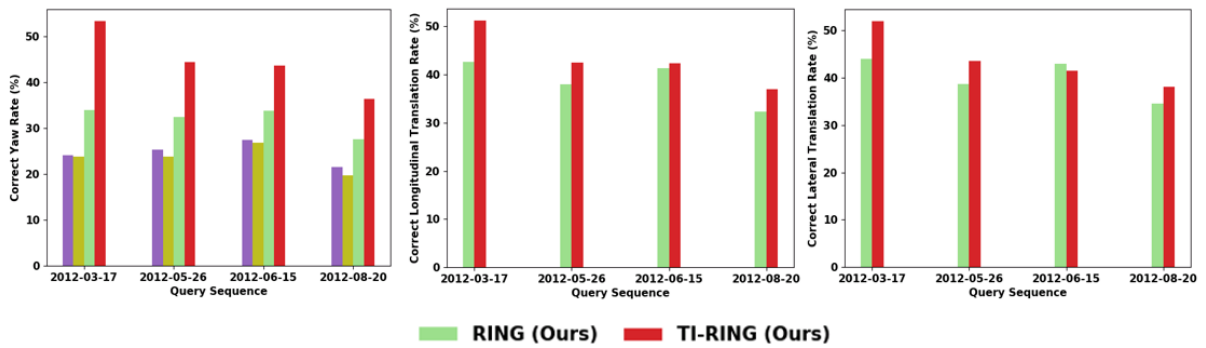


Fig. 16: Orientation and Translation Success Rate on NCLT dataset (50m place density).